# Aerosol route to $TiO_2$–$SiO_2$ catalysts with tailored pore architecture and high epoxidation activity

Valentin Smeets,[a] Cédric Boissière,[b] Clément Sanchez,[b] Eric M. Gaigneaux,[a] Elise Peeters,[c] Bert F. Sels,[c] Michiel Dusselier,[c] Damien P. Debecker[a,*]

[a] Institute of Condensed Matter and Nanosciences, Molecules, Solids, Reactivity (IMCN/MOST), UCLouvain, Place Louis Pasteur, 1, Box L4.01.09, 1348 Louvain-la-Neuve, Belgium.

[b] Sorbonne Université, CNRS, Collège de France, PSL Research University, Laboratoire Chimie de la Matière Condensée de Paris, LCMCP, 4 Place Jussieu, F-75005 Paris, France.

[c] Centre for Surface Chemistry and Catalysis, KU Leuven, Celestijnenlaan 200F, 3001 Leuven, Belgium.

*Aerosol-assisted sol-gel, epoxidation catalyst, TS-1, hierarchically porous materials, titanosilicate*

Herein, we present the aerosol-assisted sol-gel preparation of hierarchically porous $TiO_2$–$SiO_2$ catalysts having a sphere-like shell morphology and a high Ti dispersion. In order to control the porosity at the micro-, meso- and macro- levels, we use the evaporation-induced self assembly (EISA) of a surfactant, possibly combined with polymer beads as hard templates. These catalysts are tested for the epoxidation of cyclohexene with cumene hydroperoxide as oxidant, and their performance is compared to the reference TS-1 zeolite. The high catalytic performance observed with the catalysts prepared by aerosol stems from their high specific surface area, but also from the short diffusion path length generated by the meso-/macro-pore architecture which provide entryways for bulky reactants and products. Besides, these materials can incorporate a higher Ti loading than TS-1 zeolite, while ensuring a good control over the Ti speciation. Thus, the unique features of the aerosol process – which is also known to be scalable – allow us to prepare catalytic materials with high epoxidation activity, also for bulky olefins.

## 1. Introduction

The simultaneous control over active site speciation and texture is key to develop high performance heterogeneous catalysts. These parameters indeed dictate the intrinsic activity of the catalyst and the efficiency of the mass transport within the solid, and it is challenging to optimize both aspects simultaneously.

A common illustration of this dilemma is the titanium-containing zeolite TS-1 which has been industrialized in the mid-eighties as a selective oxidation catalyst.[1] More particularly, the combination of TS-1 and hydrogen peroxide $H_2O_2$ has been mainly used in two industrial applications, namely phenol hydroxylation and cyclohexanone ammoximation,[2] the latter being involved in the production of caprolactam, an important molecule used in the production of nylon 6.[3] TS-1 is also an efficient catalyst for the epoxidation of lower olefins with $H_2O_2$, even at low temperature and in the presence of water, thus bringing an environmentally friendly alternative to typical epoxidation processes (*e.g.* for propylene oxide production).[4] For these selective oxidation reactions, isolated Ti species in tetrahedral coordination are known to be the active sites.[4,5]

Despite these appealing characteristics, TS-1 suffers from two drawbacks: i) the Ti loading in the MFI crystal structure of TS-1 is commonly limited to a maximum of 2.5 % (here and after the loading is expressed as mol Ti / (mol Ti + mol Si) × 100 %)[6,7]; ii) the intrinsic microporosity of the zeolite framework is not compatible with the size of bulkier olefins – such as cyclohexene for example, oxidizing agents, and reaction products for which diffusion in and out the pores is strongly hampered.[2,8]

Extending the versatility of Ti-containing catalysts to a wider range of substrates and conditions is a challenge that can be tackled by two approaches. On the one hand, if the microporosity is assumed to be inaccessible, it is possible to enhance the activity of TS-1 by decreasing the size of the zeolite crystals so as to increase the proportion of external surface.[9] In such case, small TS-1 crystals can be advantageously dispersed at the surface of another porous solid support with the desired pore size and pore architecture. For example, Liu *et al.*[10] proposed the *in situ* hydrothermal synthesis of a hierarchically porous TS-1/modified-diatomite composite, exploited in the hydroxylation of toluene and phenol with $H_2O_2$. A similar idea is to prepare hierarchical materials based on the TS-1 structure supplemented with larger pores.[11] However, the conversion is still limited by the titanium loading and the microporosity of TS-1.

A second way out is to incorporate titanium atoms in silica-based materials with controlled texture, featuring larger pores[12,13] (*e.g.* Ti-beta zeolites,[14] Ti-MCM-41,[15] $TiO_2$–$SiO_2$ aerogels,[16,17] $TiO_2$–$SiO_2$ xerogels[18–21]). Sol-gel chemistry[22,23] represents an important toolbox for the bottom-up preparation of such mesoporous catalysts.[24,25] The most significant progress in this direction was obtained thanks to the development of templating strategies (*e.g.* evaporation-induced self-assembly, EISA[26,27]), or of specific drying strategies.[28] How-

ever, in these cases, controlling the transition metal dispersion remains a challenge owing to the different hydrolysis and condensation rates for Ti and Si precursors. This can be tackled with specific strategies, including the use of reactivity modifiers,[29,30] or non-hydrolytic routes,[31] for instance. Nevertheless, the fine tuning of the porosity at the micro-, meso- and macro- levels is still often limited by the numerous and time-consuming steps required to generate, control and preserve the pore architecture.

Currently, the aerosol-assisted sol-gel process is emerging as a versatile and highly potent method for the preparation of advanced nanomaterials,[32,33] in particular heterogeneous catalysts (**Figure 1**).[34] Such bottom-up preparation route was shown particularly powerful to control simultaneously the texture, the composition and the homogeneity of various types of mixed oxide catalysts,[35–41] including $TiO_2$–$SiO_2$ formulations.[11,42] Based on the fast drying of the aerosol precursor solution, the method exploits the quenching of the condensation kinetics, leading to highly homogeneous formulations. Besides, the porosity can be easily controlled by the incorporation of templating agents in the precursor solution.

Here, we propose to leverage on this aerosol strategy to obtain, in one step and in a continuous fashion, sphere-like particles of $TiO_2$–$SiO_2$ catalysts with both tunable hierarchical porous architecture and highly dispersed Ti species. To control the texture at different levels, we use the evaporation-induced self-assembly of a surfactant (**Figure 1a**), possibly combined with hard templates, during the aerosol process. The advantageous properties of these materials are exploited in a model epoxidation reaction and compared to the reference TS-1.

## 2. Experimental Section

### 2.1. Preparation of the materials

The catalysts were prepared with a 4 % Ti loading starting from precursor solutions prepared as follow:

**Aer_15**. For 1 g of calcined material, 0.231 g titanium butoxide (TiBuO, Fluka, 99%) was first added dropwise to 1.257 g 40% (w/w) aqueous tetrapropylammonium hydroxide (TPAOH, Merck) under stirring. After 10 min mixing, 5.196 g deionized $H_2O$ were added, followed by 10 min stirring and the subsequent addition of 3.357 g tetraethyl orthosilicate (TEOS, Sigma). The resulting solution was kept overnight under vigorous stirring to hydrolyse the precursors and further aged for 15h at 70°C in a closed vessel. 0.989 g of Pluronic® F127 (BASF) were then added and the solution was thoroughly mixed for at least 1h. The composition of the resulting clear yellowish solution was 1 $SiO_2$: 0.042 $TiO_2$: 0.16 TPAOH: 0.005 F127: 17 $H_2O$: 4 EtOH. **Aer_15_2%.** The precursor solution was prepared by the same procedure using 0.116 g TiBuO, 1.262 g 40% aq. TPAOH, 5.218 g deionized $H_2O$, 3.441 g TEOS and 0.993 g F127. The final composition was 1 $SiO_2$: 0.02 $TiO_2$: 0.15 TPAOH: 0.005 F127: 16 $H_2O$: 4 EtOH.

**Aer_20**. The precursor solution was prepared using 0.231 g TiBuO, 1.676 g 40% aq. TPAOH, 4.946 g deionized $H_2O$, 3.358 g TEOS and 0.989 g F127. The final composition was 1 $SiO_2$: 0.042 $TiO_2$: 0.21 TPAOH: 0.005 F127: 17 $H_2O$: 4 EtOH.

**Aer_25**. The precursor solution was prepared using 0.231 g TiBuO, 2.091 g 40% aq. TPAOH, 4.686 g deionized $H_2O$, 3.352 g TEOS and 0.987 g F127. The final composition was 1 $SiO_2$: 0.042 $TiO_2$: 0.26 TPAOH: 0.005 F127: 17 $H_2O$: 4 EtOH.

The precursor solutions were sprayed by a Büchi Mini Spray Dryer B-290 with an air pressure of 4 bars. The aerosol was dried by passing through a glass reactor heated at 220°C (**Aer_15**, **Aer_20** and **Aer_25**) or 75°C (**Aer_PS** and **Aer_PMMA**). The obtained powders were aged at 70°C overnight and then calcined in air at 550°C for 5 h (5°C/min).

Monodisperse colloidal suspension of PMMA was prepared following a surfactant-free synthesis using ammonium peroxodisulfate as thermal initiator according to the procedure of Goodwin *et al.*[43] The synthesis was carried out at 90°C in a double envelop reactor thermostated with a waterbath circulation. After synthesis, the colloidal suspension was filtered through filter paper in order to remove few particles aggregates produced onto the edge of the reactor. So obtained PMMA latex exhibits a mean particle size distribution centered at 278 nm (with FWHM of 63 nm).

Monodisperse PS colloidal suspension was obtained following an emulsion polymerization route initiated by potassium persulfate initiator and sodium dihexylsulfosuccinate according to the procedure of Blas *et al.*[44] The average particle size measured by DLS was 95 nm (FWHM 10 nm).

**Aer_PS** and **Aer_PMMA** were obtained after mixing 11.75 g of the same precursor solution as **Aer_20** with respectively 86 g of PS (7.9 % w/w) and 188 g of PMMA (3.6% w/w) latex. The resulting suspension was mixed for 30 min before spray-drying procedure.

A reference **TS-1** catalyst was prepared with a Ti loading of 1.8% by hydrothermal synthesis according to a procedure adapted from the literature,[7] using titanium isopropoxide and tetraethyl orthosilicate as Ti and Si sources, respectively. The detailed preparation procedure is available in the Supporting Information.

### 2.2. Characterization of the materials

The Ti content of the materials was measured by ICP-AES on an ICP 6500 instrument (Thermo Scientific Instrument) after dissolution of the samples by sodium peroxide fusion. XPS experiments were carried out using an SSX 100/206 spectrometer (Surface Science Instruments, USA) with Al-Kα radiation operated at 10 kV and 20 mA. The binding energy scale was calibrated on the Si 2p peak, fixed at 103.5 eV.[45] The quantification of Ti in Ti–O–Si and Ti–O–Ti was based on the decomposition of the $2p_{3/2}$ peak at approximately 460.0 and 458.5 eV, respectively.[46,47] Si was quantified on the basis of the Si 2p peak at 103.5 eV.[45] Powder X-ray diffraction (PXRD) patterns were recorded at room temperature on a Siemens D5000 diffractometer equipped with a Ni filter using CuKα radiation (Bragg-Brentano geometry) operated at 40 kV and 40 mA. Diffractograms were taken between 5° and 80° (2θ) with a step size of 0.02° (2θ). The band gap energy ($E_g$) values of **Aer_15** and **Aer_15_2%** were calculated from the optical absorption edge on DR UV-VIS spectra recorded on an Agilent Cary 5000 UV-VIS-NIR spectrophotometer at room temperature in 4000–50000 $cm^{-1}$ range. The pelletized samples (250–500 µm) were loaded into the U-tube, equipped with a UV-VIS transparent window. Before measurement, the samples were dried at 300°C under $N_2$ for 1h with a heating rate of 5°C.$min^{-1}$. After drying, the samples were kept under $N_2$ during measurement. $BaSO_4$ pellets (250–500 µm), dried according to the same procedure, were used to measure the background spectra. The DR UV-VIS spectra were background corrected and the Kulbelka Munk function was used to display the data. Other spectra were recorded on a Varian Cary 5000

UV–Vis–NIR Spectrophotometer with a Harrick single-beam Praying Mantis Diffuse Reflectance collection system. The spectra were recorded at room temperature in 12500–50000 cm-1 range. Spectralon® Diffuse Reflectance Standard was used to measure the background spectra. The DR UV-VIS spectra were background corrected and the Kulbelka Munk function was used to display the data. Scanning electron microscopy (SEM) images were taken using a JEOL 7600F microscope at 15 kV voltage. Samples were pre-treated with a chromium sputter coating of 15 nm carried out under vacuum with a Sputter Metal 208 HR (Cressington). SEM-FEG pictures were obtained with a Hitachi SU-70. Textural properties were determined from $N_2$ adsorption/desorption isotherms at -196°C using a Tristar 3000 instrument (Micromeritics, USA). Prior to measurement, the samples were first degassed overnight under vacuum at 150°C. The pore size distribution was obtained from the adsorption branch using the BJH method. The specific surface area was evaluated by the BET method in the relative pressure range of 0.01–0.1 for the aerosol catalysts and 0.01–0.05 for **TS-1**, in order to take into account the presence of micropores.[48] The micropore volume and micropore specific surface area were evaluated by the t-plot method in the thickness range of 3.5–5.0 Å.

### 2.3. Catalytic activity

The catalytic properties were investigated for the epoxidation of cyclohexene with cumene hydroperoxide as the oxidizing agent. The reaction was carried out in a two-necked glass round-bottomed reactor at 90°C, equipped with a condenser, a magnetic stirrer and a rubber septum. In a typical run, 0.765 g (0.9 mol.l$^{-1}$) cyclohexene (Sigma-Aldrich, 99%), 0.065 g (0.05 mol.l$^{-1}$) nonane (TCI, > 98%) – used as the internal standard – and 50 mg (5 g.l$^{-1}$) catalyst were pre-mixed in 7.468 g of water saturated toluene (*ca.* 330 ppm $H_2O$) under stirring. After 10 min, 0.342 g (0.18 mol.l$^{-1}$) of cumene hydroperoxide (Sigma, 80%) was added and the mixture was allowed to react for 3h. The product formation was followed by collecting aliquots at regular time intervals and by analysing them in gas chromatography, using a Varian CP-3800 chromatograph equipped with a FID detector and a capillary column (BR-5, 30 m, 0.32 mm i.d., 1.0 µm film thickness). Catalyst recyclability has been assessed on four consecutive measurements on the same catalyst powder. After each catalytic test, the catalyst was recovered by centrifugation, dried overnight at 120°C under vacuum and calcined at 550°C for 5h (5°C/min). The hot filtration test was carried out by removing the catalyst by filtration after 30 min reaction time; the filtrated reaction mixture was then allowed to react for an additional 2h30 min.

## 3. Results and discussion

### 3.1. Preparation of the materials

The aerosol process[34] consists in atomizing a precursor solution, containing the gel precursors, into small droplets which are dispersed inside a carrier gas (*i.e.* aerosol) and processed by passing through a heated zone (**Figure 1b**). In those conditions, the solvent evaporates and the gel quickly condenses and dries, forming solid microspheres. In typical conditions (see the experimental section), we expected the formation of spherical particles with a hollow morphology (**Figure 1 c**). The titanium loading was set at 4 % in all experiments, which is considerably higher than that in typical TS-1.

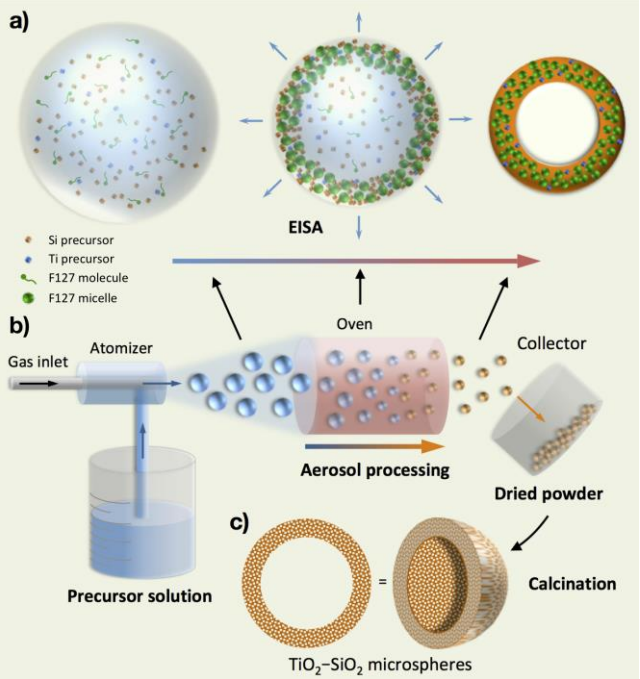


**Figure 1.** Preparation of mesostructured $TiO_2$–$SiO_2$ microspheres by a so-called Type IIIc aerosol technique.[34] a) Illustration of the evaporation-induced self-assembly (EISA) mechanism (TPAOH has been omitted for clarity); b) Schematic representation of the aerosol set-up; c) Illustration of the texture and morphology of the calcined material in the typical conditions used (see the experimental section for further details).

Macro- and meso-porosity were designed by the use of two types of templating agents (**Figure 2**): (i) Pluronic® F127, a block copolymer surfactant that forms micelles via evaporation-induced self-assembly (EISA)[49] and (ii) stable colloidal suspensions of polystyrene (PS) or poly (methyl methacrylate) (PMMA) polymer beads. The use of tetrapropylammonium hydroxide (TPAOH) ensures the hydrolysis of the titanium precursor and favours $Ti^{4+}$ incorporation in tetrahedral sites. Concomitantly, micropores were also formed in all materials, due to the incorporation of $TPA^+$ cations in the inorganic framework. Although these micropores are not relevant for the conversion of large molecules, their presence demonstrates how we can easily tune the porosity and obtain hierarchical porous materials.

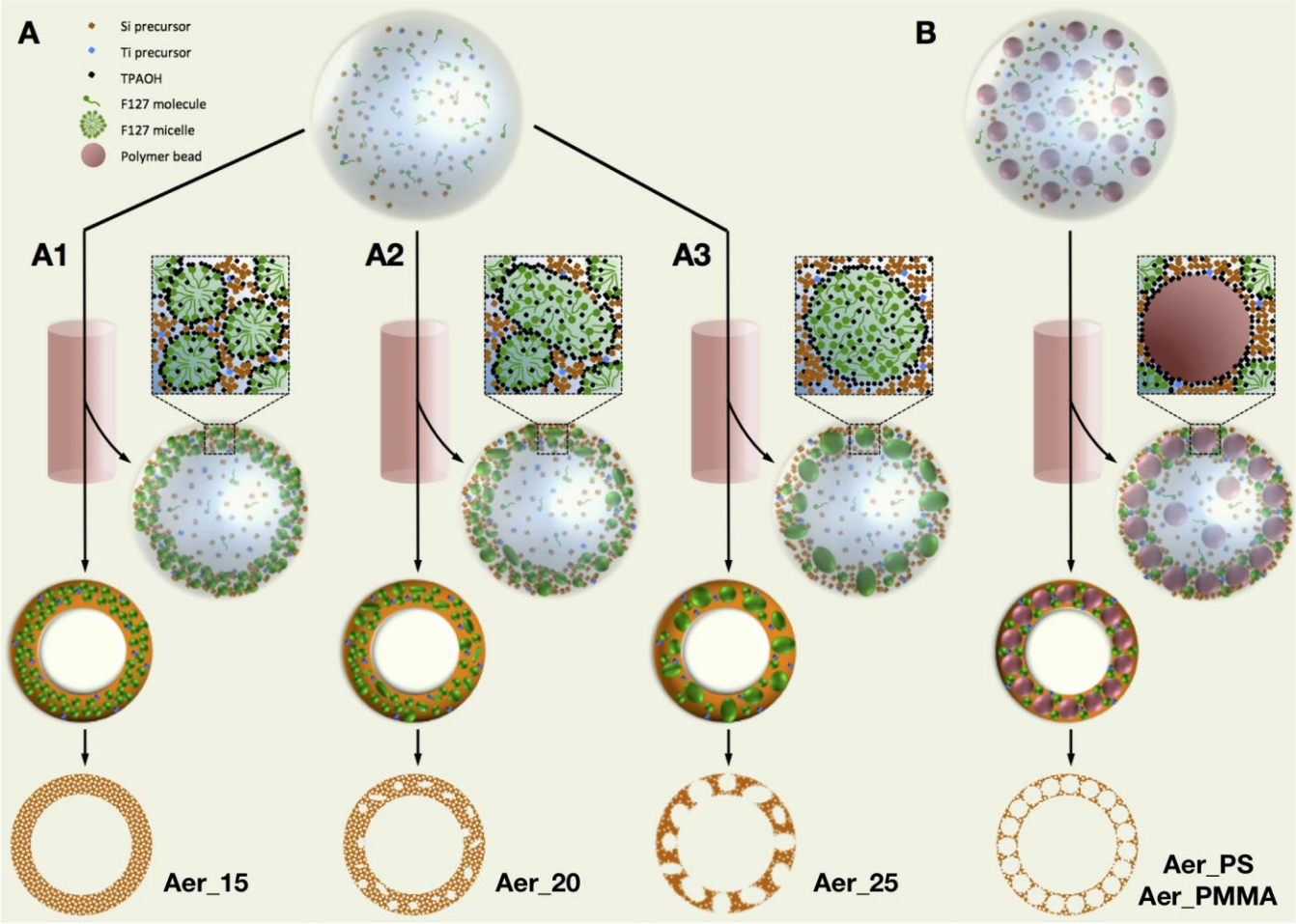


**Figure 2.** Schematic representation of the routes used for the preparation of $TiO_2$–$SiO_2$ with tailored porosity. In "Route A", the porosity was controlled by increasing the TPAOH to (Si+Ti) molar ratio, which allows to move from a mesoporous material formed by an evaporation-induced self-assembly mechanism (Route A1) to a macroporous solid resulting from a phase separation mechanism (Routes A2 and A3). In "Route B", macropores were generated by a hard-templating approach using polymer beads of various sizes.

Route A (**Figure 2**) corresponds to the use of F127 surfactant molecules and TPAOH as templating agents. During the aerosol processing, the gel precursors condensed around the self-assembled micelles of surfactant, which are known to form spherical structure of about 6 nm in diameter.[50] However, in addition to the role of micro-structuring agent of TPAOH, it was previously reported that $TPA^+$ cations are partitioned between the inorganic walls and the F127 micelles, where it plays a role of swelling agent (at low amount), and phase separating agent (at high amount).[37] We thus expected the formation of large mesopores above 6 nm from its use. As a consequence, in a first preparation, we used a F127 to Si molar ratio of 0.005 and a TPAOH to (Si+Ti) molar ratio of 0.15 to prepare a dual micro-meso-structured material (Route A1, **Figure 2**). After calcination, to remove the organics and release the porosity, the material was denoted "**Aer_15**".

Variation of the TPAOH amount can be used to tune the pore size of mixed oxides, as it was recently reported for the preparation of aluminosilicates acid catalysts with large pores.[37] By increasing the TPAOH to (Si+Ti) molar ratio in the precursor solution to 0.20 and 0.25 (resp. Route A2 and Route A3, **Figure 2**), the pH increased and the condensation rate of the precursors decreased. Besides, the swelling effect of $TPA^+$ was amplified as more cations were incorporated in the organic phase. In those conditions, a phase separation was initiated, since the interactions between the organic and inorganic phases became too low to stabilize the mesostructure by EISA.[37,51] In the typical conditions of spray-dry processing, this metastable system has been quenched before it reached the thermodynamic equilibrium, corresponding to a complete phase separation.[52] Using a TPAOH to (Si+Ti) molar ratio of 0.20, we obtained a material with a heterogeneous porosity resulting from the early transition between EISA and phase separation. This material was denoted "**Aer_20**". When the amount of TPAOH was the highest (*i.e.* TPAOH/(Si+Ti) = 0.25), the material, denoted "**Aer_25**", almost presented a dual micro-macro-porosity, with only a small proportion of mesopores in the material (see **Figure 2** and textural analysis below).

Although this strategy is appealing to tailor the porosity at micro-, meso- and macro-scales, the control over the macroporosity is not straightforward whenever phase separation is involved; for instance, the temperature gradient in the heating part of the spray-drying apparatus may produce variable drying time and thus large macropore size distributions. So, in Route B (**Figure 2**) PS (95 ± 10 nm FWHM) or PMMA (278 ± 63 nm FWHM) polymer beads were used as hard templates to prepare alternative and well-controlled porous materials with three-level micro-meso-macro-structure.[43,44] The latex were thoroughly mixed with the same precursor solution as **Aer_20** and spray-dried at 75°C, thus lower than the glass

transition temperature of the polymers (*ca.* 95°C for PS and *ca.* 105°C for PMMA). The final composition of the precursor solution allowed the incorporation of the polymer beads in a close-packing arrangement. The materials were named "**Aer_PS**" and "**Aer_PMMA**".

### 3.2. Characterization of the materials

Elemental analysis (**Table 1**) showed that the experimental bulk Ti content was close to the nominal content for all catalysts. This result demonstrates an excellent control over the bulk composition, with a quantitative incorporation of both titanium and silicon species in the final material.

**Table 1. Percentage of Ti species (mol Ti / (mol Ti + mol Si) × 100 %) in the catalysts (bulk composition, ICP-AES) and at the catalysts surface (from XPS)**

| | Bulk Ti %[a] | Surf. Ti % | Surf. Ti–O–Si % | % Ti–O–Si[b] |
|---|---|---|---|---|
| **TS-1** | 1.6 (1.8) | 1.3 | 1.2 | 90 |
| **Aer_15** | 4.0 (4.0) | 3.3 | 2.8 | 85 |
| **Aer_20** | 4.7 (4.0) | 4.2 | 3.5 | 85 |
| **Aer_25** | 4.8 (4.0) | 4.3 | 3.6 | 84 |
| **Aer_PS** | -[c] | 3.8 | 3.3 | 85 |
| **Aer_PMMA** | -[c] | 3.5 | 3.0 | 84 |

[a]Nominal composition (corresponding to the precursor solution) is given in brackets. [b]% Ti–O–Si = (Surf. Ti–O–Si % / Surf. Ti %) × 100. [c]Not measured in ICP-AES; materials obtained with the same precursor solution as **Aer_20**.

XPS analyses were conducted in order to investigate the surface composition and the quality of the Ti dispersion at the surface (**Table 1**, see also **Figure S1**, Supporting Information). For all aerosol catalysts, the surface Ti concentration is close to the bulk content, showing that the aerosol method leads to homogeneous mixed oxide particle compositions, as there is no relative enrichment of the surface with Si or Ti oxide.

Among the Ti detected at the surface of the catalyst by XPS, one can distinguish the fraction that is truly incorporated into the silica matrix (denoted "Ti–O–Si" in **Table 1**) from the fraction that is not dispersed and is instead present as extra-framework Ti–O–Ti species. The former is found at *ca.* 460.0 eV and the latter is found at *ca.* 458.5 eV.[46,47] The Ti 2p peak deconvolution is shown in **Figure S1** for all catalysts. In TS-1, it is well known that almost all surface Ti atoms are incorporated in the well-defined crystalline framework. Indeed, the results show a proportion of well-dispersed surface Ti atoms of 90% for this sample. These isolated Ti sites are known to be the active epoxidation species.[4,5] Importantly, aerosol-made catalysts show a similar excellent dispersion (**Table 1**). Moreover, the absolute amount of dispersed Ti–O–Si at the surface is twice as high as for **TS-1**, in line with the corresponding higher Ti loading (*viz.* ~4 *vs.* 1.8 %).

PXRD analyses indicated that the aerosol catalysts are all amorphous (**Figure S2**, Supporting Information). No evidence of the presence of a $TiO_2$ crystalline phase, such as anatase with characteristic reflection at $2\theta = 25°$, was found, which excludes the presence of $TiO_2$ crystallites larger than 5 nm. The **TS-1** reference catalyst showed the expected diffraction pattern, typical for its MFI structure.[7]

The high dispersion of Ti in aerosol catalysts is further confirmed by the maximum absorption band in the 210–225 nm range on the DRUV-vis spectra of the catalysts, which corresponds to Ti atoms in tetrahedral coordination (**Figure 3**).[53] The small contribution above 250 nm could be characteristic of the presence of small amounts of Ti in higher coordination number, for instance due to water coordination, local oligomeric Ti species or small $TiO_2$ nanodomains.[53–55] However, no evidence of the presence of a crystalline phase such as anatase, having a maximum characteristic absorption around 330 nm,[56] could be found in the spectra.

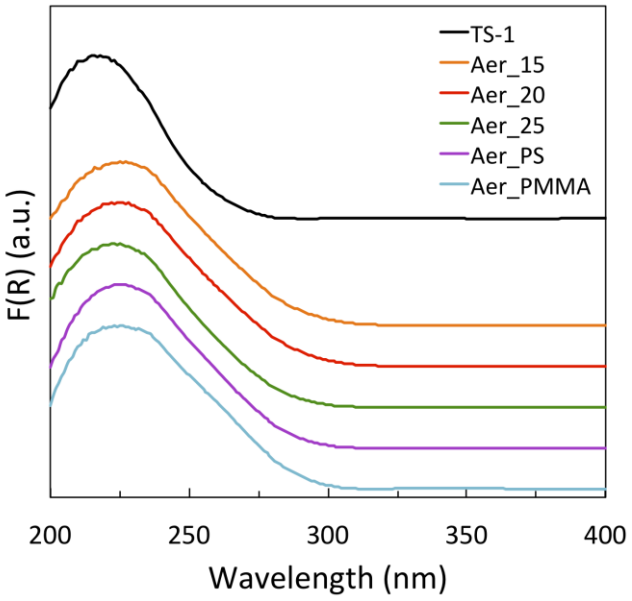


**Figure 3.** DRS UV-visible spectra of the catalysts (Kubelka-Munk Function).

SEM and SEM-FEG images of the mixed oxides are shown in **Figure 4** (route A) and **Figure 5** (route B). The $TiO_2$–$SiO_2$ microspheres are in the 1–20 μm size range and mainly show a hollow spherical structure with some distortion. Images in **Figure 4** unravel the effect of the amount of TPAOH on the pore size. **Aer_15** shows a regular porous structure with small mesopores clearly visible in the SEM-FEG image (**Figure 4d**). **Aer_20** presents the same type of pores at the external surface, but shows also the characteristic structure of an early stage phase separation, with discernible large pores formed mainly on the inner side of the shell (**Figure 4e**). By comparison, **Aer_25** reached a more advanced state of phase separation which strongly affected the meso-structuration of the material. For this catalyst, macropores as large as 200 nm are clearly distinguishable at the surface (**Figure 4 f**).

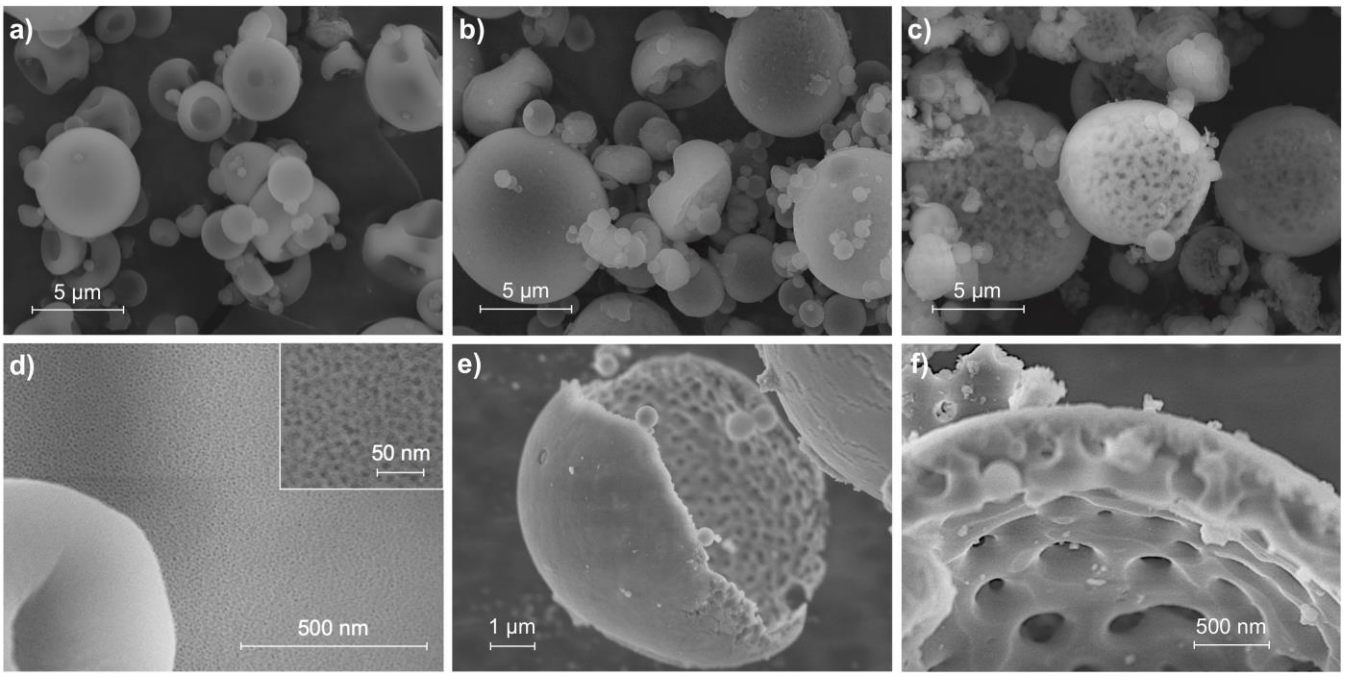


**Figure 4.** SEM (a–c) and SEM-FEG (d–f) images of **Aer_15** (a, d), **Aer_20** (b, e) and **Aer_25** (c, f).

Alternatively, macropores have been formed using polymer beads as sacrificial template. The same kind of distorted hollow structures are observed (**Figure 5**). SEM-FEG confirms that the beads, which were removed by calcination, were in a close-packing arrangement during the formation of the solid. The macropore dimensions are *ca.* 80 nm and 150–200 nm for **Aer_PS** and **Aer_PMMA**, respectively, in line with the template size. The small shrinkage of the macropores observed for **Aer_PMMA** may be attributed to a partial hydrolysis of the PMMA side chains into polyacrylic acid under basic conditions.[57]

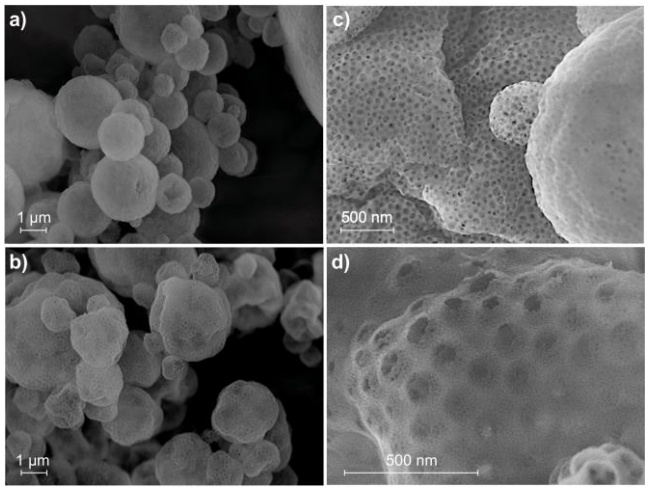


**Figure 5.** SEM (a–b) and SEM-FEG (c–d) images of **Aer_PS** (a, c) and **Aer_PMMA** (b, d).

**Table 2. Textural properties of the aerosol catalysts compared to the reference material TS-1**

| | $S_{BET}$ ($m^2.g^{-1}$) | $S_{\mu}$ ($m^2.g^{-1}$)[a] | $V_p$ ($cm^3.g^{-1}$)[b] | $V_{\mu}$ ($cm^3.g^{-1}$)[a] |
|---|---|---|---|---|
| **TS-1** | 510 | 380 | 0.43 | 0.15 |
| **Aer_15** | 640 | 380 | 0.79 | 0.16 |
| **Aer_20** | 630 | 450 | 0.48 | 0.18 |
| **Aer_25** | 620 | 450 | 0.38 | 0.19 |
| **Aer_PS** | 520 | 370 | 0.45 | 0.15 |
| **Aer_PMMA** | 890 | 380 | 0.80 | 0.15 |

[a]Micropore specific surface area and micropore volume calculated from the t-plot (see **Figure S3**, Supporting Information). [b]Measured at $P/P_0 = 0.98$.

$N_2$-physisorption isotherms are shown in **Figure 6**, along with the BJH pore size distributions. The presence of mesopores in all aerosol samples is evidenced by the type IV isotherms, which are typically observed for mesoporous solids. Textural data are summarized in **Table 2**. As expected, **TS-1** solely displayed micropores and interparticular spaces which contribute to the total pore volume. In comparison, much higher total pore volumes and BET specific surface areas were obtained by the aerosol method, whereas the micropore volumes and the micropore specific surface areas were in the same range. Subtracting the microporous component, all aerosol catalysts thus have higher specific surface areas and pore volumes compared to **TS-1**, and are therefore expected to facilitate the conversion of large molecules.

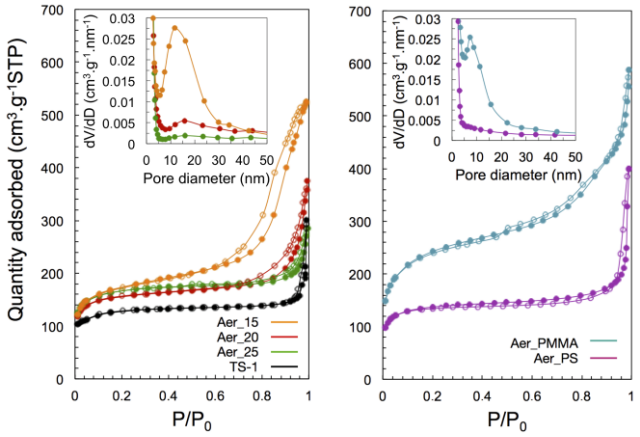


**Figure 6.** $N_2$ adsorption-desorption isotherms of the $TiO_2$–$SiO_2$ mixed oxides prepared by aerosol with different templates: F127 surfactant with various TPAOH to (Si+Ti) molar ratios (left); PS and PMMA polymer beads (right). Pore size distributions (PSD) based on the adsorption branch are shown in inset. The isotherm of microporous **TS-1** is shown for comparison. Full symbols are used for the adsorption isotherms and empty symbols are used for the desorption isotherms.

Pore size distributions of **Aer_15**, **Aer_20** and **Aer_25** are centred at *ca.* 15 nm (inset, **Figure 6**). This pore size should be related to the formation of swollen F127 micelles, whose diameter has been increased by the incorporation of $TPA^+$ cations.[37] By increasing the TPAOH amount, this swelling effect is amplified and leads to the disruption of the micelles, likely explaining a part of the phase separation phenomenon.[51] **Aer_20** and **Aer_25** therefore present a lower mesostructuration, as evidenced by the shape of the isotherms (**Figure 6**). Nevertheless, the BET specific surface areas remain comparable (**Table 2**).

**Aer_PS** and **Aer_PMMA** appear to have lower micropore volumes (**Table 2**). This could be explained by strong interactions between the polymer chains and $TPA^+$ cations, which could tend to adsorb at the surface of the polymer beads and therefore be unavailable to act as the structuring agent (see Route B, **Figure 2**). For the same reason, the role of $TPA^+$ cations as swelling agent is compromised, resulting in lower mesopore size for **Aer_PMMA** (*ca.* 10 nm). In the case of **Aer_PS**, such mesopores are absent and we assume that the close packing of the PS beads creates inorganic walls which are too thin to accommodate the F127 micelles. It must be noted that the BET specific surface area of **Aer_PMMA** is comparatively high (890 $m^2.g^{-1}$); this appears to be due to the presence of additional mesopores smaller than 3.8 nm. Although not appearing clearly on the adsorption branch PSD (inset, **Figure 6**), these pores can be evidenced by the forced closure of the isotherm upon desorption at $P/P_0$ value of 0.4–0.5 due to the tensile strength effect (TSE) and visualized on the desorption branch PSD (see **Figure S4**, Supporting Information).[58] These small mesopores may result from the interpenetration of linear polymer chains within the inorganic phase.

### 3.3. Catalytic performance

The materials were tested in batch mode for the epoxidation of cyclohexene. Using hydrogen peroxide (30% w/w aqueous solution) as the oxidant, the aerosol catalysts showed much higher epoxidation activity as compared to **TS-1** (**Figure S5** and **Table S1**). Yet, we observed a *ca.* 50% activity loss after four consecutive tests carried out on **Aer_20** catalyst, whereas **TS-1** kept the same activity (**Figure S6**). In fact, it is generally accepted that amorphous mixed oxides are sensitive to the presence of water,[59] which constitutes a certain limitation to our aerosol-made catalysts.

Thus, the epoxidation of cyclohexene was investigated in organic conditions, using cumene hydroperoxide (CHP) as the oxidant. A hot filtration test was carried out, confirming that all the catalytic activity was attributable only to the solid material (see **Figure S7**).

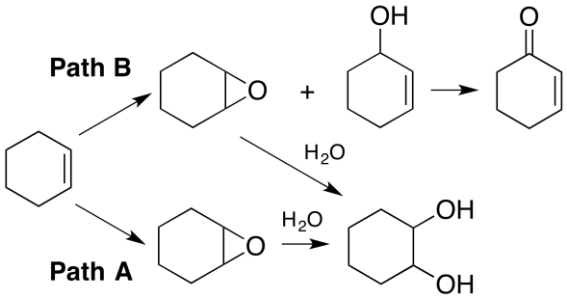


**Figure 7.** Reaction scheme for the epoxidation of cyclohexene. Path A refers to direct epoxidation pathway; Path B refers to radical oxidation pathway.

In addition to the targeted epoxide formation by direct epoxidation pathway (Path A, **Figure 7**), the reaction scheme for cyclohexene oxidation reveals the possible formation of other products, including cyclohexane diol, formed by the epoxide ring-opening, as well as 2-cyclohexen-1-ol and its oxidation product 2-cyclohexen-1-one, formed by an unwanted radical oxidation pathway (Path B, **Figure 7**).

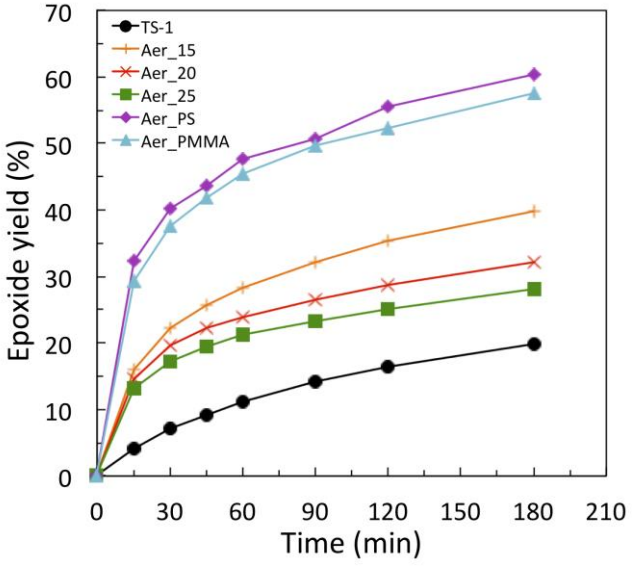


**Figure 8.** Kinetic data for the conversion of cyclohexene into cyclohexene oxide in toluene using cumene hydroperoxide (CHP) as oxidizing agent. Experimental conditions: T = 90°C, [CATA] = 5 $g.l^{-1}$, [Cyclohexene] = 0.9 $mol.l^{-1}$, [CHP] = 0.18 $mol.l^{-1}$.

**Table 3. Yield (Y), selectivity (S) and initial turnover frequency (TOF) for Ti-catalyzed cyclohexene epoxidation at 90°C (3h) with cumene hydroperoxide**

| | $Y_{Epox}$ (%)[a] | $Y_{Diol}$ (%)[a] | $Y_{Alcohol}$ (%)[a] | $Y_{Ketone}$ (%)[a] | $X_{CHP}$ (%) | $S_{Epox}$ (%) | PB $S_{Epox}$ (%)[b] | TOF ($h^{-1}$)[c] |
|---|---|---|---|---|---|---|---|---|
| **TS-1** | 20 | <1 | 3 | 0 | 16 | 123 | 86 | 37 |
| **Aer_15** | 40 | 2 | 0 | <1 | 45 | 87 | 94 | 48 |
| **Aer_15_2%** | 46 | 2 | 0 | <1 | 51 | 90 | 96 | 122 |
| **Aer_20** | 32 | 2 | 0 | <1 | 37 | 88 | 94 | 36 |
| **Aer_25** | 28 | 2 | 0 | <1 | 30 | 93 | 93 | 30 |
| **Aer_PS** | 60 | 1 | 0 | <1 | 63 | 96 | 97 | 89 |
| **Aer_PMMA** | 58 | 3 | 0 | <1 | 65 | 89 | 95 | 83 |

[a]The yields are expressed as the amount of product formed divided by the initial amount of CHP. Epox = cyclohexene oxide, Diol = cyclohexane diol, Alcohol = 2-cyclohexen-1-ol, Ketone = 2-cyclohexen-1-one. [b]Product-based selectivity; these values have been calculated by dividing the epoxide yield by the overall yield instead of the CHP conversion. [c]Initial TOF approximated from the CHP conversion at 15 min reaction time. It is defined as the number of mole of CHP converted per minute divided by the number of active sites (deduced from "Surf. Ti–O–Si %", **Table 1**); one example of TOF calculation is shown in the Supporting Information.

Under the experimental conditions depicted in **Figure 8**, our catalysts present a much higher epoxide yield compared to **TS-1**. From **Table 3**, all aerosol catalysts also present a higher CHP conversion compared to the reference zeolite. Comparison among the catalysts is also presented in terms of initial TOF, approximated by the CHP conversion at the early stage of the reaction (15 min). The selectivity toward the epoxide reaches 87 to 96% for the aerosol catalysts (**Table 3**), the remaining gap in product selectivity being mainly explained by the hydrolysis of the epoxide to form cyclohexane diol.

In the case of **TS-1**, almost no cyclohexane diol is formed, consistent with the fact that the intrinsic hydrophobicity of the zeolite might repel water molecules from the catalyst surface.[5] However, the selectivity toward the epoxide – defined as the amount of epoxide formed divided by the amount of CHP consumed – is found to be higher than 100%. In fact, we found that the same reaction, carried out in the absence of CHP, leads to a production of epoxide and 2-cyclohexen-1-ol in similar amounts. Actually, molecular oxygen was already reported to be able to trigger the radical oxidation pathway (Path B, **Figure 7**) in the epoxidation of cyclohexene.[60] Therefore, we interpret the unrealistic selectivity value obtained for **TS-1** in the light of a non-selective and CHP independent formation of the epoxide. This interpretation is further supported by the presence of a significant amount of 2-cyclohexen-1-ol in this case (**Table 3**). Interestingly, the non-selective oxidation of cyclohexene seems to only occur on **TS-1** since no 2-cyclohexen-1-ol and almost no 2-cyclohexen-1-one are found in the case of the aerosol catalysts, which all appear to operate via the direct epoxidation pathway only (Path A, **Figure 7**).

The higher catalytic activity obtained with the aerosol catalysts can be ascribed to two key features: i) the higher amount of well-incorporated Ti at the catalyst surface, and ii) the texture and pore architecture, with a higher specific surface area compared to **TS-1** zeolite associated with the presence of accessible mesopores. To discriminate between these two possible explanations, we synthesized an aerosol catalyst with a nominal Ti loading of 2 % (bulk) – closer to that of **TS-1** – while keeping the same gel composition as **Aer_15** ("**Aer_15_2%**"). In terms of texture, this catalyst was very similar to **Aer_15**, with a BET specific surface area of 790 $m^2.g^{-1}$, a pore volume of 0.87 $cm^3.g^{-1}$, and a similar pore size distribution (see **Figure S8**). The experimental surface Ti–O–Si content determined by XPS was 1.3 %, similar to **TS-1** (1.2 %). **Aer_15_2%** had an initial TOF about three times higher when compared to **TS-1** (**Table 3**). This is a strong indication of the positive impact of the hierarchical texture of the aerosol catalyst on the activity, allowing faster molecular transport through the catalyst. Interestingly, the overall yield and selectivity of **Aer_15_2%** is similar to that of **Aer_15,** despite a two times lower Ti content and comparable texture. This translates into more than twofold higher initial TOF for **Aer_15_2%**. Calculating the band gap energy ($E_g$) of the catalysts from the optical absorption edges in the DR UV-vis spectra obtained in dehydrated conditions[61–63] (see **Figure S9**), we found that the value of $E_g$ for **Aer_15_2%** (4.75 eV) is higher than for **Aer_15** (4.50 eV). The higher $E_g$ value of **Aer_15_2%** is related to a relatively higher proportion of isolated tetrahedral Ti species, which contributes to the increase in the epoxidation rate per surface Ti site.

The catalysts prepared by aerosol, having the same Ti loading and similar Ti speciation, reached different levels of activity. This is tentatively correlated with their textural properties. For **Aer_25**, **Aer_20** and **Aer_15**, the activity tends to increase as the specific surface area increases and as the microporous specific surface area decreases, pointing to a possible beneficial effect of increasing the accessible surface area. The much higher performance reached by **Aer_PS** and **Aer_PMMA** does not seem to be fully explained by a high accessible surface area. Although this should be verified by dedicated experiments on diffusion phenomena, we suggest that the macroporosity created by the close packing of polymer beads facilitates mass transport phenomena, owing to the thinness of the walls that separate the macropores.[64]

A recyclability study carried out on **Aer_20** revealed that there was only a *ca.* 20% decrease of the catalytic activity over four consecutive tests (**Figure 9**), much less than for the same catalyst tested in the presence of aqueous solution of $H_2O_2$. This small decrease could be associated to the presence of small amounts of water in the solvent and potentially could be further improved by working under strict non aqueous conditions.[21] Also, a $N_2$ physisorption analysis carried out on **Aer_20** and **TS-1** after the four consecutive cycles revealed a *ca.* 25% decrease of the BET specific surface area and pore volume for the aerosol catalyst (490 $m^2.g^{-1}$, 0.37 $cm^3.g^{-1}$),

whereas the BET specific surface area and pore volume of **TS-1** were not affected (550 $m^2.g^{-1}$, 0.40 $cm^3.g^{-1}$). This result suggests that the decrease in activity for the aerosol catalyst may also be due to a surface loss upon repetitive reaction cycles, and could be avoided by optimizing the recycling procedure.

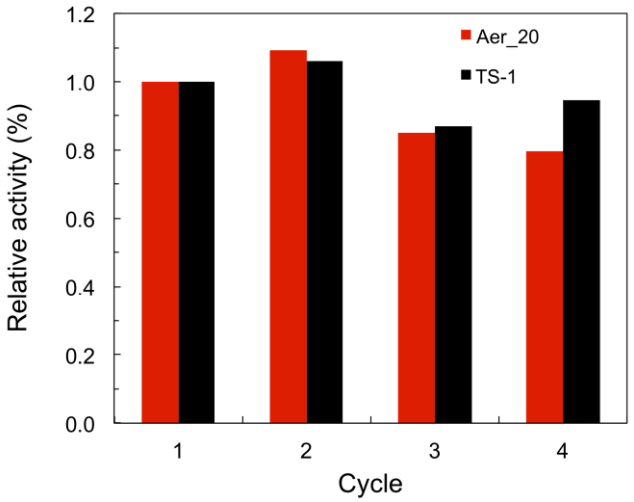


**Figure 9.** Recyclability study of the **TS-1** and **Aer_20** catalysts with CHP as oxidant. Data were collected in the initial stage of the reaction (15 min reaction time) and the catalytic activity (expressed in terms of CHP conversion) relative to the first test was calculated for each catalyst. The composition was identical to **Figure 8**.

## 4. Conclusions

In this paper, we demonstrated that the aerosol technique is a powerful technology for the preparation of $TiO_2$–$SiO_2$ mixed oxides possessing a variety of pore sizes and architectures, while controlling simultaneously the composition, homogeneity and dispersion of the titanium species. High specific surface areas with large pores in the meso- and macro-porous range were reached. These latter characteristics stand for the higher catalytic performance of these materials for the epoxidation of cyclohexene compared to TS-1. Though these materials can accommodate a higher Ti loading than typical TS-1 zeolite, the increasing titanium loading was shown not to lead to a substantial increase of the epoxidation performance (TOF), as it results in higher Ti coordination.

$TiO_2$–$SiO_2$ prepared by aerosol processing have a high potential for the synthesis of bulkier and highly valuable epoxides (*e.g.* alpha-pinene oxide, norbonene oxide, linalool oxide) potentially in continuous flow mode, since the particle size should permit the design of a fixed bed reactor. Besides, it should be reminded that such aerosol process can easily be scaled-up, thus meeting requirements for future industrial applications.

## ASSOCIATED CONTENT

### Supporting Information

Detailed procedure for the preparation of the reference TS-1 catalyst; XPS Ti 2p spectra; PXRD patterns; t-plots; pore size distribution on desorption of **Aer_PMMA**; catalytic tests in the presence of hydrogen peroxide and recyclability study; hot filtration test of **Aer_20**; $N_2$ adsorption-desorption isotherm, pore size distribution and t-plot of **Aer_15_2%**; estimation of the band gap energy values of **Aer_15_2%** and **Aer_15**; example of calculation of the initial TOF value for **Aer_15**.

## AUTHOR INFORMATION

### Corresponding Author

*E-mail : damien.debecker@uclouvain.be (D.P. Debecker)

## ACKNOWLEDGMENT

Authors acknowledge the 'Communauté française de Belgique' for the financial support through the ARC programme (15/20-069). F. Devred is acknowledged for the technical and logistical support. V. Smeets is thankful to F.R.S.–F.N.R.S for his FRIA PhD grant. The authors thank the Francqui Foundation for the chair, which made it possible for Prof. Sanchez to visit Belgium. FEGSEM instrumentation was facilited by the Institut des Matériaux de Paris Centre (IMPC FR2482) and was funded by UPMC, CNRS and by the C'Nano projects of the Région Ile-de-France. Elise Peeters acknowledges funding by an FWO SB-fellowship.

## REFERENCES

(1) Taramasso, M.; Perego, G.; Notari, B. Preparation of Porous Crystalline Synthetic Material Comprised of Silicon and Titanium Oxides. US4410501A, October 18, 1983.

(2) Perego, C.; Carati, A.; Ingallina, P.; Mantegazza, M. A.; Bellussi, G. Production of Titanium Containing Molecular Sieves and Their Application in Catalysis. *Appl. Catal. A* **2001**, *221* (1), 63–72.

(3) Fisher, W. B.; Crescentini, L.; Staff, U. by. Caprolactam. In *Kirk-Othmer Encyclopedia of Chemical Technology*; American Cancer Society, 2015; pp 1–11.

(4) Clerici, M. G.; Ingallina, P. Epoxidation of Lower Olefins with Hydrogen Peroxide and Titanium Silicalite. *J. Catal.* **1993**, *140* (1), 71–83.

(5) Clerici, M. G. The Activity of Titanium Silicalite-1 (TS-1): Some Considerations on Its Origin. *Kinet. Catal.* **2015**, *56* (4), 450–455.

(6) Millini, R.; Previde Massara, E.; Perego, G.; Bellussi, G. Framework Composition of Titanium Silicalite-1. *J. Catal.* **1992**, *137* (2), 497–503.

(7) Thangaraj, A.; Eapen, M. J.; Sivasanker, S.; Ratnasamy, P. Studies on the Synthesis of Titanium Silicalite, TS-1. *Zeolites* **1992**, *12* (8), 943–950.

(8) Murugavel, R.; Roesky, H. W. Titanosilicates: Recent Developments in Synthesis and Use as Oxidation Catalysts. *Angew. Chem. Int. Ed. Engl.* **1997**, *36* (5), 477–479.

(9) Zuo, Y.; Liu, M.; Zhang, T.; Meng, C.; Guo, X.; Song, C. Enhanced Catalytic Performance of Titanium Silicalite-1 in Tuning the Crystal Size in the Range 1200–200 Nm in a Tetrapropylammonium Bromide System. *ChemCatChem* **2015**, *7* (17), 2660–2668.

(10) Liu, H.; Lu, G.; Guo, Y.; Guo, Y.; Wang, J. Deactivation and Regeneration of TS-1/Diatomite Catalyst for Hydroxylation of Phenol in Fixed-Bed Reactor. *Chem. Eng. J.* **2005**, *108* (3), 187–192.

(11) Guo, Z.; Xiong, G.; Liu, L.; Li, P.; Hao, L.; Cao, Y.; Tian, F. Aerosol-Assisted Synthesis of Hierarchical Porous Titanosilicate Molecular Sieve as Catalysts for Cyclohexene Epoxidation. *J. Porous Mater.* **2016**, *23* (2), 407–413.

(12) Corma, A. From Microporous to Mesoporous Molecular Sieve Materials and Their Use in Catalysis. *Chem. Rev.* **1997**, *97* (6), 2373–2419.

(13) Vansant, E. F. Pore Size Engineering in Zeolites. In *Studies in Surface Science and Catalysis*; Grobet, P. J., Mortier, W. J., Vansant, E. F., Schulz-Ekloff, G., Eds.; Innovation in Zeolite Materials Science; Elsevier, 1988; Vol. 37, pp 143–153.

(14) Camblor, M. A.; Corma, A.; Martínez, A.; Pérez-Pariente, J. Synthesis of a Titaniumsilicoaluminate Isomorphous to Zeolite Beta and Its Application as a Catalyst for the Selective Oxidation of Large Organic Molecules. *J. Chem. Soc., Chem. Commun.* **1992**, *0* (8), 589–590.

(15) Blasco, T.; Corma, A.; Navarro, M. T.; Pariente, J. P. Synthesis, Characterization, and Catalytic Activity of Ti-MCM-41 Structures. *J. Catal.* **1995**, *156* (1), 65–74.

(16) Hutter, R.; Mallat, T.; Baiker, A. Titania Silica Mixed Oxides: II. Catalytic Behavior in Olefin Epoxidation. *J. Catal.* **1995**, *153* (1), 177–189.

(17) Dutoit, D. C. M.; Schneider, M.; Baiker, A. Titania-Silica Mixed Oxides: I. Influence of Sol-Gel and Drying Conditions on Structural Properties. *J. Catal.* **1995**, *153* (1), 165–176.

(18) Smeets, V.; Ben Mustapha, L.; Schnee, J.; Gaigneaux, E. M.; Debecker, D. P. Mesoporous SiO2-TiO2 Epoxidation Catalysts: Tuning Surface Polarity to Improve Performance in the Presence of Water. *Mol. Catal.* **2018**, *452*, 123–128.

(19) Lafond, V.; Mutin, P. H.; Vioux, A. Control of the Texture of Titania−Silica Mixed Oxides Prepared by Nonhydrolytic Sol−Gel. *Chem. Mater.* **2004**, *16* (25), 5380–5386.

(20) Cojocariu, A. M.; Mutin, P. H.; Dumitriu, E.; Fajula, F.; Vioux, A.; Hulea, V. Mild Oxidation of Bulky Organic Compounds with Hydrogen Peroxide over Mesoporous TiO2-SiO2 Xerogels Prepared by Non-Hydrolytic Sol–Gel. *Appl. Catal. B* **2010**, *97* (3–4), 407–413.

(21) Lorret, O.; Lafond, V.; Mutin, P. H.; Vioux, A. One-Step Synthesis of Mesoporous Hybrid Titania−Silica Xerogels for the Epoxidation of Alkenes. *Chem. Mater.* **2006**, *18* (20), 4707–4709.

(22) Brinker, C. J.; Scherer, G. W. *Sol-Gel Science: The Physics and Chemistry of Sol-Gel Processing*; Academic Press, 2013.

(23) Livage, J.; Sanchez, C. Sol-Gel Chemistry. *J. Non-Crystalline Solids* **1992**, *145*, 11–19.

(24) Debecker, D. P. Innovative Sol-Gel Routes for the Bottom-up Preparation of Heterogeneous Catalysts. *Chem. Rec.* **2017**.

(25) Landau, M. V. Sol–Gel Process. In *Handbook of Heterogeneous Catalysis*; American Cancer Society, 2008; pp 119–160.

(26) Brinker, C. J.; Lu, Y.; Sellinger, A.; Fan, H. Evaporation-Induced Self-Assembly: Nanostructures Made Easy. *Adv. Mater.* **1999**, *11* (7), 579–585.

(27) Zhong, R.; Peng, L.; de Clippel, F.; Gommes, C.; Goderis, B.; Ke, X.; Tendeloo, G. V.; Jacobs, P. A.; Sels, B. F. An Eco-Friendly Soft Template Synthesis of Mesostructured Silica-Carbon Nanocomposites for Acid Catalysis. *ChemCatChem* **2015**, *7* (18), 3047–3058.

(28) Schneider, M.; Baiker, A. Aerogels in Catalysis. *Catal. Rev.* **1995**, *37* (4), 515–556.

(29) Livage, J.; Henry, M.; Sanchez, C. Sol-Gel Chemistry of Transition Metal Oxides. *Progr. Solid State Chem.* **1988**, *18* (4), 259–341.

(30) Sanchez, C.; Livage, J.; Henry, M.; Babonneau, F. Chemical Modification of Alkoxide Precursors. *J. Non-Crystalline Solids* **1988**, *100* (1), 65–76.

(31) Debecker, D. P.; Mutin, P. H. Non-Hydrolytic Sol–Gel Routes to Heterogeneous Catalysts. *Chem. Soc. Rev.* **2012**, *41* (9), 3624–3650.

(32) Boissiere, C.; Grosso, D.; Chaumonnot, A.; Nicole, L.; Sanchez, C. Aerosol Route to Functional Nanostructured Inorganic and Hybrid Porous Materials. *Adv. Mater.* **2011**, *23* (5), 599–623.

(33) Nandiyanto, A. B. D.; Okuyama, K. Progress in Developing Spray-Drying Methods for the Production of Controlled Morphology Particles: From the Nanometer to Submicrometer Size Ranges. *Adv. Powder Technol.* **2011**, *22* (1), 1–19.

(34) Debecker, D. P.; Le Bras, S.; Boissière, C.; Chaumonnot, A.; Sanchez, C. Aerosol Processing: A Wind of Innovation in the Field of Advanced Heterogeneous Catalysts. *Chem. Soc. Rev.* **2018**, *47* (11), 4112–4155.

(35) Maksasithorn, S.; Praserthdam, P.; Suriye, K.; Debecker, D. P. Preparation of Super-Microporous WO3–SiO2 Olefin Metathesis Catalysts by the Aerosol-Assisted Sol–Gel Process. *Microporous and Mesoporous Mater.* **2015**, *213*, 125–133.

(36) Debecker, D. P.; Stoyanova, M.; Colbeau-Justin, F.; Rodemerck, U.; Boissière, C.; Gaigneaux, E. M.; Sanchez, C. One-Pot Aerosol Route to MoO3-SiO2-Al2O3 Catalysts with Ordered Super Microporosity and High Olefin Metathesis Activity. *Angew. Chem. Int. Ed.* **2012**, *51* (9), 2129–2131.

(37) Pega, S.; Boissière, C.; Grosso, D.; Azaïs, T.; Chaumonnot, A.; Sanchez, C. Direct Aerosol Synthesis of Large-Pore Amorphous Mesostructured Aluminosilicates with Superior Acid-Catalytic Properties. *Angew. Chem. Int. Ed.* **2009**, *48* (15), 2784–2787.

(38) Wang, C. Y.; Bai, H. Aerosol Processing of Mesoporous Silica Supported Bimetallic Catalysts for Low Temperature Acetone Oxidation. *Catal. Today* **2011**, *174* (1), 70–78.

(39) Jung, K. Y.; Jung, Y. R.; Jeon, J.-K.; Kim, J. H.; Park, Y.-K.; Kim, S. Preparation of Mesoporous V2O5/TiO2 via Spray Pyrolysis and Its Application to the Catalytic Conversion of 1, 2-Dichlorobenzene. *J. Ind. Eng. Chem.* **2011**, *17* (1), 144–148.

(40) Kuai, L.; Geng, J.; Chen, C.; Kan, E.; Liu, Y.; Wang, Q.; Geng, B. A Reliable Aerosol-Spray-Assisted Approach to Produce and Optimize Amorphous Metal Oxide Catalysts for Electrochemical Water Splitting. *Angew. Chem. Int. Ed.* **2014**, *53* (29), 7547–7551.

(41) Vivian, A.; Fusaro, L.; Debecker, D. P.; Aprile, C. Mesoporous Methyl-Functionalized Sn-Silicates Generated by the Aerosol Process for the Sustainable Production of Ethyl Lactate. *ACS Sus. Chem. Eng.* **2018**, *6* (11), 14095–14103.

(42) Sachse, A.; Hulea, V.; Kostov, K. L.; Marcotte, N.; Boltoeva, M. Y.; Belamie, E.; Alonso, B. Efficient Mesoporous Silica–Titania Catalysts from Colloidal Self-Assembly. *Chem. Commun.* **2012**, *48* (86), 10648–10650.

(43) Goodwin, J. W.; Hearn, J.; Ho, C. C.; Ottewill, R. H. Studies on the Preparation and Characterisation of Monodisperse Polystyrene Latices. *Colloid Polymer Sci.* **1974**, *252* (6), 464–471.

(44) Blas, H.; Save, M.; Pasetto, P.; Boissière, C.; Sanchez, C.; Charleux, B. Elaboration of Monodisperse Spherical Hollow Particles with Ordered Mesoporous Silica Shells via Dual Latex/Surfactant Templating: Radial Orientation of Mesopore Channels. *Langmuir* **2008**, *24* (22), 13132–13137.

(45) Jacquemin, M.; Genet, M. J.; Gaigneaux, E. M.; Debecker, D. P. Calibration of the X-Ray Photoelectron Spectroscopy Binding Energy Scale for the Characterization of Heterogeneous Catalysts: Is Everything Really under Control? *ChemPhysChem* **2013**, *14* (15), 3618–3626.

(46) Erdem, B.; Hunsicker, R. A.; Simmons, G. W.; Sudol, E. D.; Dimonie, V. L.; El-Aasser, M. S. XPS and FTIR Surface Characterization of TiO2 Particles Used in Polymer Encapsulation. *Langmuir* **2001**, *17* (9), 2664–2669.

(47) Reddy, B. M.; Chowdhury, B.; Smirniotis, P. G. An XPS Study of the Dispersion of MoO3 on TiO2–ZrO2, TiO2–SiO2, TiO2–Al2O3, SiO2–ZrO2, and SiO2–TiO2–ZrO2 Mixed Oxides. *Appl. Catal. A* **2001**, *211* (1), 19–30.

(48) Rouquerol, J.; Llewellyn, P.; Rouquerol, F. Is the Bet Equation Applicable to Microporous Adsorbents? In *Studies in Surface Science and Catalysis*; Llewellyn, P. L., Rodriquez-Reinoso, F., Rouqerol, J., Seaton, N., Eds.; Characterization of Porous Solids VII; Elsevier, 2007; Vol. 160, pp 49–56.

(49) Lu, Y.; Fan, H.; Stump, A.; Ward, T. L.; Rieker, T.; Brinker, C. J. Aerosol-Assisted Self-Assembly of Mesostructured Spherical Nanoparticles. *Nature* **1999**, *398* (6724), 223–226.

(50) Godard, N.; Vivian, A.; Fusaro, L.; Cannavicci, L.; Aprile, C.; Debecker, D. P. High-Yield Synthesis of Ethyl Lactate with Mesoporous Tin Silicate Catalysts Prepared by an Aerosol-Assisted Sol–Gel Process. *ChemCatChem* **2017**, *9* (12), 2211–2218.

(51) Areva, S.; Boissière, C.; Grosso, D.; Asakawa, T.; Sanchez, C.; Lindén, M. One-Pot Aerosol Synthesis of Ordered Hierarchical Mesoporous Core–Shell Silica Nanoparticles. *Chem. Commun.* **2004**, *0* (14), 1630–1631.

(52) Chaumonnot, A.; Tihay, F.; Coupé, A.; Pega, S.; Boissière, C.; Grosso, D.; Sanchez, C. New Aluminosilicate Materials with Hierarchical Porosity Generated by Aerosol Process. *Oil Gas Sci. Technol.* **2009**, *64* (6), 681–696.

(53) Bini, F.; Rosier, C.; Saint-Arroman, R. P.; Neumann, E.; Dablemont, C.; de Mallmann, A.; Lefebvre, F.; Niccolai, G. P.; Basset, J.-M.; Crocker, M.; et al. Surface Organometallic Chemistry of Titanium: Synthesis, Characterization, and Reactivity of ( ⋮ Si−O)NTi(CH2C(CH3)3)4-n (n = 1, 2) Grafted on Aerosil Silica and MCM-41. *Organometallics* **2006**, *25* (15), 3743–3760.

(54) Marchese, L.; Maschmeyer, T.; Gianotti, E.; Coluccia, S.; Thomas, J. M. Probing the Titanium Sites in Ti−MCM41 by Diffuse Reflectance and Photoluminescence UV−Vis Spectroscopies. *J. Phys. Chem. B* **1997**, *101* (44), 8836–8838.

(55) Marchese, L.; Gianotti, E.; Dellarocca, V.; Maschmeyer, T.; Rey, F.; Coluccia, S.; Thomas, J. M. Structure–Functionality Relationships of Grafted Ti-MCM41 Silicas. Spectroscopic and Catalytic Studies. *Phys. Chem. Chem. Phys.* **1999**, *1* (4), 585–592.

(56) Madhusudan Reddy, K.; Manorama, S. V.; Ramachandra Reddy, A. Bandgap Studies on Anatase Titanium Dioxide Nanoparticles. *Mater. Chem. Phys.* **2003**, *78* (1), 239–245.

(57) Thanoo, B. C.; Jayakrishnan, A. Preparation of Hydrogel Beads from Crosslinked Poly(Methyl Methacrylate) Microspheres by Alkaline Hydrolysis. *J. Appl. Polymer Sci.* **1990**, *39* (5), 1153–1161.

(58) Groen, J. C.; Peffer, L. A. A.; Pérez-Ramírez, J. Pore Size Determination in Modified Micro- and Mesoporous Materials. Pitfalls and Limitations in Gas Adsorption Data Analysis. *Microporous Mesoporous Mater.* **2003**, *60* (1), 1–17.

(59) Deo, G.; Turek, A. M.; Wachs, I. E.; Huybrechts, D. R. C.; Jacobs, P. A. Characterization of Titania Silicalites. *Zeolites* **1993**, *13* (5), 365–373.

(60) Jorda, E.; Tuel, A.; Teissier, R.; Kervennal, J. Synthesis, Characterization, and Activity in the Epoxidation of Cyclohexene with Aqueous H2O2 of Catalysts Prepared by Reaction of TiF4with Silica. *J. Catal.* **1998**, *175* (1), 93–107.

(61) Gao, X.; Bare, S. R.; Fierro, J. L. G.; Banares, M. A.; Wachs, I. E. Preparation and In-Situ Spectroscopic Characterization of Molecularly Dispersed Titanium Oxide on Silica. *J. Phys. Chem. B* **1998**, *102* (29), 5653–5666.

(62) De Clercq, R.; Dusselier, M.; Poleunis, C.; Debecker, D. P.; Giebeler, L.; Oswald, S.; Makshina, E.; Sels, B. F. Titania-Silica Catalysts for Lactide Production from Renewable Alkyl Lactates: Structure–Activity Relations. *ACS Catal.* **2018**, 8130–8139.

(63) De Clercq, R.; Dusselier, M.; Makshina, E.; Sels, B. F. Catalytic Gas-Phase Production of Lactide from Renewable Alkyl Lactates. *Angew. Chem. Int. Ed.* **2018**, *57* (12), 3074–3078.

(64) Hartmann, M.; Machoke, A. G.; Schwieger, W. Catalytic Test Reactions for the Evaluation of Hierarchical Zeolites. *Chem. Soc. Rev.* **2016**, *45* (12), 3313–3330.